biophysica

MDPI

Article

Emergence of Gloomy Eyelet inside DNA

Jean-Marc Sabatier [1,*] and Farzan Amini [2]

[1] Institute of Neurophysiopathology (INP)-UMR 7051, Faculté des Sciences Médicales et Paramédicales, Aix-Marseille University, 27, Bd Jean Moulin, 13005 Marseille, France
[2] exERT, Bd Pierre Dramard, 13015 Marseille, France
* Correspondence: sabatier.jm1@libertysurf.fr

Abstract: The purpose of this article is to study gloomy eyelet (GE) inside the cell nucleus by using models of warp drive hydro (WDH), swinging spring, Rankine, co-moving reference frame, and Poincare. The beat wave frequency (ω) of blood pressure on the vessel and the swinging spring frequency (Ω) of DNA coincide together on the Rankine model. In this case, it leads to appearing as a sudden pressure drop and an accelerated cavity in the medium of the warp drive hydro (WDH) model. In transient conditions, the vortex flow inside WDH can generate gloomy eyelet (GE), and the tiny distortion of nano space–time revealed inside the gloomy eyelet (GE) inside DNA and the tiny distortion of nano space–time revealed inside the co-moving reference frame (CMRF) model of the gloomy eyelet (GE). The space–time distortion can act as a hidden potential for the cell nucleus and some behaviors of gloomy eyelet can be traced by the frequency responses of human body organs. The interactions between two adjacent different mediums such as the normal cells and abnormal cells, earth's gravitational effects can lead to changes in the distortion of space–time inside the cell nucleus. Transient bonds between particles can be expected to appear in the gloomy eyelet inside DNA. Identifying the range of changes in the frequency responses and the transient bonds inside the cell nucleus can be introduced as one of the health indicators.

Keywords: gloomy eyelet (GE); warp drive hydro (WDH) model; swinging spring model; co-moving reference frame (CMRF); Rankine model; pseudo-spherical geometry; space–time; sudden pressure drop; accelerated cavity

Citation: Sabatier, J.-M.; Amini, F. Emergence of Gloomy Eyelet inside DNA. *Biophysica* **2023**, *3*, 35–45. https://doi.org/10.3390/biophysica3010003

Academic Editor: Jaume Casademunt

Received: 18 November 2022
Revised: 3 January 2023
Accepted: 12 January 2023
Published: 20 January 2023

1. Introduction

The speed of sound in normal human tissues varies significantly; it ranges from roughly 1430 m/s in breast tissue to 1647 m/s in muscle (Gyongy and Kollar 2015; Mamou and Oelze 2013). Despite this variation, clinical ultrasound scanners typically use an assumed speed of sound (1540 m/s) for image reconstruction. A second and perhaps more important result of the ability to accurately and consistently predict the speed of sound in vivo lies in tissue characterization. The longitudinal speed of sound is often affected by tissue pathology. Consider, for example, the diagnosis of non-alcoholic fatty liver disease (NAFLD), which is characterized by diffuse infiltration of fat into the hepatocytes of the liver. The normal liver has approximately 5% fat content; this may increase to above 30% in advanced cases of steatosis. Fat has a relatively lower longitudinal speed of sound than healthy liver tissue. Consequently, the expected speed of sound in a fatty liver will be lower than that in a healthy liver.

Speed of sound estimation is relevant in the field of breast imaging and early detection of breast cancer. Breast density, as assessed by mammograms, reflects breast tissue composition (Boyd et al., 2010). The breast has a relatively low longitudinal speed of sound (~1430 m/s) as it is primarily composed of fat. However, breast tumors have higher sound speeds and tend to cause increases in the bulk speed of sound (Boyd et al., 2010). Consequently, the ability to predict the longitudinal speed of sound in vivo is of importance in the longitudinal monitoring of breast health. Furthermore, knowledge of the speed

of sound within the tumor and the surrounding breast tissue can greatly aid ultrasound image-guided radiation treatment (IGRT), wherein an accurate speed of sound estimate can be used to better define and visualize the target (tumor or lesion) [1].

Examples of propagation velocities in different tissues are such as air: 330 m/s, fat: 1450 m/s, water: 1480 m/s, liver: 1550 m/s, kidney: 1560 m/s, blood: 1570 m/s, muscle: 1580 m/s, bone: 4080 m/s.

In the human body, particles and nanobubbles can reach more than the higher speed in transient conditions and while passing through different environments, which create special conditions in the downstream environment. This new environment has features that are examined in this article. For this investigation, we propose the relative motion by Warp Drive Hydro (WDH).

2. Materials and Methods

2.1. Natural and Vortex Frequencies of Cell

The natural frequencies of any kind of cells are dependent on physical characteristics and for this reason, those are individual. The changes in the frequency of tumor cells are subject to the stiffness of the tumor cell, the Mode shape of 2ND of cell is shown in Figure 1.

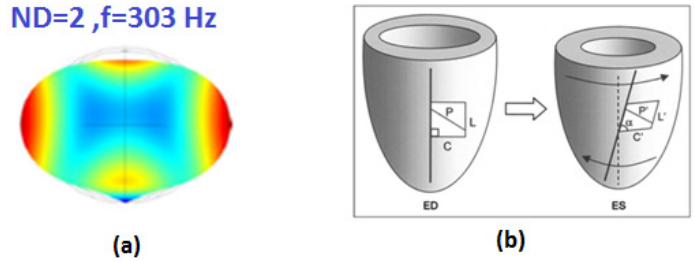

Figure 1. (**a**) Natural frequency of typical cell; (**b**) the rotation of left ventricular with speed (Ω).

When the material is deformed (stretched, perhaps), energy (usually referred to as strain energy) is stored in the deformation of its bonds, and it is this energy that brings the material back to its original shape—or perhaps not, since that energy can be dissipated in a number of ways, such as heat, sound, surface energy, plastic deformation, or kinetic energy. With a Hookean material, the strains are relatively small, and all the energy is stored in stretching the interatomic bonds, termed the internal energy. However, if the material is made of relatively long and unrestrained molecules, the energy can also be stored in changes in their shape and mobility, termed entropic energy [2].

Perfusion and diffusion are two mechanisms by which inert and metabolic gases exchange between tissue and blood. Perfusion denotes the blood flow rate in simplest terms, while diffusion refers to the gas penetration rate in tissue, or across tissue– blood boundaries [3].

The potential for tribonucleation, bubble growth, or collapse in the blood flow is considered under sinusoidal and steady shear flow [4].

The pulsatile blood flow and wall motion are based on physiological velocity and vessel motion waveforms. The results demonstrate that the oxygen transport in coronary arteries is altered by wall motion and indicate that the degree of influence depends on individual motion patterns [5].

2.2. Left Ventricular Torsion

Left ventricular torsion has long been recognized as a characteristic of normal mammalian cardiac function, described by William Harvey and many others. Relative to end-diastole (ED) the apex of the left ventricle rotates anticlockwise about its central axis, as viewed from the apex, at a relatively constant rate throughout systole, to a maximum value of ~10°. The base, initially rotating anticlockwise, reverses direction to give a net clockwise rotation by end-systole (ES) of ~3°. The resulting end-systolic torsion (defined to be positive by convention) is often described as being similar to wringing out a wet towel.

During diastole, much of the systolic torsion is released during isovolumic relaxation, due to the mechanical recoil of elastic energy built up during systole. Thus, relaxation of torsion is a direct measure of the deactivation of myocytes and release of stored elastic energy, both of which facilitate rapid filling.

2.3. Pressure Drop

The predictions of the strain-based and stress-based are compared on a homogenous blood flow that superimposes steady and sinusoidal shearing described by:

$$G(t) = \frac{du_x}{dy} = G_0(1 + \sin(wt)), \tag{1}$$

where $G(t)$ and λ are sinusoidal shear rate and eigenvalue, accordingly. Therefore, the periodic deformation of bubbles could occur in blood flow when they are subjected to sinusoidal shear flow. The excess pressure drop resulting from the presence of a single leukocyte is calculated for various values of hematocrit and vessel diameter. When the adherent leukocytes are spaced far enough, they act as independent particles. In this case, the total excess pressure drop due to their combined effect is simply the sum of the individual contributions [2,5],

$$\Delta P_{et} = n\Delta P_e \quad , \tag{2}$$

3. Main Models

3.1. Swinging Spring Model

Nonlinear spatial vibrations of a mass point on a weightless elastic suspension (pendulum on a spring) are considered. The frequency of vertical vibrations is assumed to be equal to the doubled swinging frequency (the 1:1:2 resonance),

In this case, as numerical calculations and experiments show, the vertical vibrations are unstable, which leads to the vertical vibration energy transfer to the pendulum swinging energy. The vertical vibrations of the mass point decay and, after a certain time period, the pendulum starts swinging in a certain vertical plane. This swinging is also unstable, which results in the reverse energy transfer into the vertical vibration mode. The swing spring model has been presented in Figure 2.

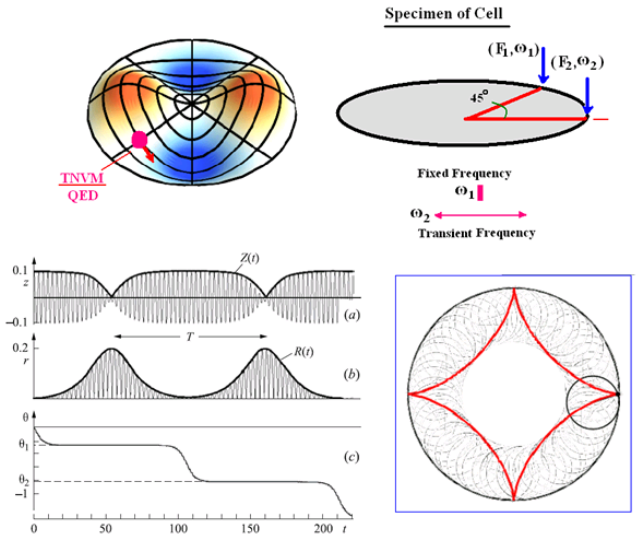

Figure 2. Swinging spring model generated by two excitation forces; (**a**) the amplitude of the springing component and (**b**) the amplitude of the swinging component and (**c**) the angle of swinging component.

The vertical vibrations are again repeated. However, after the second transfer of the vertical vibration energy to the pendulum swinging energy, the apparent plane of vibrations rotates by a certain angle [6,7].

For a circular plate, the mode shapes of modes with nodal lines can be rotated by using two excitation signals at different locations at the outer edge with a certain phase and space difference. The superposition of the two standing waves results in a traveling wave and can be observed in a rotating mode shape. The circular cell is chosen for studying and exerting the excitation forces, while the swinging spring model is made on the circular plate (as the forced vortex region of the Rankine model), those are facing resonance frequency [8,9].

3.2. Rankine Model and Acceleration Model

The particular case of the rotating mode shape is possible to change pressure and velocity suddenly in Rankine Model. The resonance conditions in this model have been studied as below:

Under the Special condition $\beta(t) = \omega(t)$, it is possible for the swinging spring model to appear and pressure drop will be a function of acceleration. If we face this condition, a sudden pressure drop, and accelerated cavity will occur [10–12].

$$\frac{\partial v_r}{\partial r} + \frac{v_r}{r} + \frac{\partial v_z}{\partial z} = 2\beta - \alpha = 0 \quad (r \leq R_0 - \delta), \tag{3}$$

$$\frac{\partial v_\varphi}{\partial t} + v_r \frac{\partial v_\phi}{\partial r} + \frac{v_r v_\phi}{r} = r\left(\frac{d\omega}{dt} - 2\beta\omega(t)\right) = 0, \tag{4}$$

3.3. Poincare Model on WDH

The aim of this part is to consider the infinity medium on the pseudo-spherical trajectory and warp drive hydro (WDH) model by suing the Poincare model. In mathematics, non-Euclidean geometry consists of two geometries based on axioms closely related to those specifying Euclidean geometry. As Euclidean geometry lies at the intersection of metric geometry and affine geometry, non-Euclidean geometry arises when either the metric requirement is relaxed, or the parallel postulate is replaced with an alternative one. In the latter case, one obtains hyperbolic geometry and elliptic geometry, the traditional non-Euclidean geometries. When the metric requirement is relaxed, then there are affine planes associated with the planar algebras which give rise to kinematic geometries that have also been called non-Euclidean geometry. The essential difference between the metric geometries is the nature of parallel lines. Another way to describe the differences between these geometries is to consider two straight lines indefinitely extended in a two-dimensional plane that are both perpendicular to a third line:

- In Euclidean geometry, the lines remain at a constant distance from each other (meaning that a line drawn perpendicular to one line at any point will intersect the other line and the length of the line segment joining the points of intersection remains constant) and are known as parallels.
- In hyperbolic geometry, they "curve away" from each other, increasing in distance as one moves further from the points of intersection with the common perpendicular; these lines are often called ultra-parallels.
- In elliptic geometry, the lines "curve toward" each other and intersect.

The Lobachevski plane is the plane obtained by removing the fifth Euclid axiom on parallels and which is replaced by a point outside a line, there are at least two parallels to that line. The points of the circle of radius 1 are the points at infinity and this circle is called the absolute. The lines are the chords of the circle. We can see that point M pass two parallels to line m.

Hyperbolic geometry is a form of non-Euclidean geometry that replaces the parallel postulate of Euclidean geometry. There are four models in hyperbolic geometry: Poincare the Disk Model, the Klein Model, the Poincare half-plane model, and the Hyperboloid [13].

3.4. Warp Drive Hydro (WDH) Model

It is a part of the hyperbolic plane if we regard the surface as flat and geodesic as a straight line. This surface is one possibility in the attempt of immersing the Lobachevski plane in 3D Euclidean space. A pseudo-sphere is a surface of revolution of the Tractrix curve and is the generator of the surface of revolution of the pseudo-sphere.

According to the Rankine model, the curve of pressure drop in the vortex flow is like a Pseudo-sphere geometry. Most points of the curve of pressure drop are placed on the Pseudo-sphere curve:

- Since the trace are obtained in a finite amount of time and distance, this means that the "point at infinity" maybe is not so much at an infinite distance.
- Such pseudo-spheres generally (not always) have points at infinity which are due to the non-immersiblity of the Lobochevski plane into the 3D Euclidean space.

There are an infinite number of particles at an infinitesimal scale at the pseudo-sphere of the pressure drop curve [13].

A sudden pressure drop in the pseudo-sphere geometry on the Rankine model can create a warp drive hydro (WDH) model. As mentioned above, an infinity medium can assume the warp drive hydro model.

4. Gloomy Eyelet inside WDH Model

4.1. Beat Frequency on the Pressure Vessel

Working in the opposite sense to attenuation is the fact that the radius decreases, and the elasticity of the arterial walls decrease towards the peripheral circulation. These features are, respectively, known as radial taper and elastic taper. Their effect in increasing the speed of propagation of the pulse pressure wave has been noted. They also produce a gradual increase in the characteristic impedance along an unbranched length of the vessel.

The effect of non-linearity is the opposite, to increase the pulsatility of the waveform by moving energy from low frequency harmonics into higher-frequency ones. The result of this is to increase the steepness of the systolic rise so that the peak moves towards the start of the systole. The pressure and velocity waveforms have been shown in Figure 3.

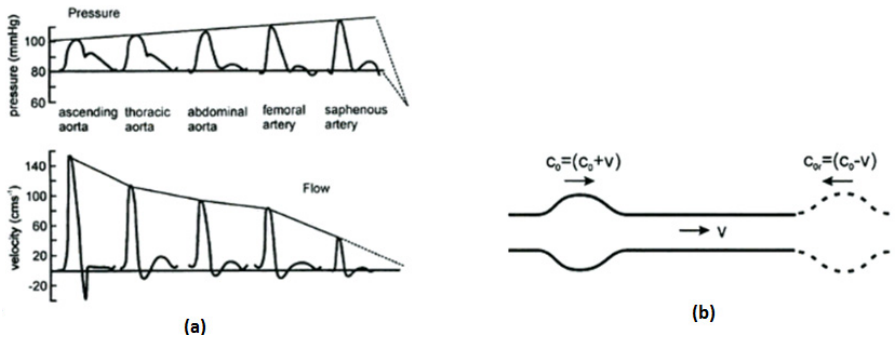

Figure 3. (**a**) Pressure and velocity waveforms in arteries as they travel away from the heart adapted from measurements made in dogs. The waveforms show the effects of amplification of the pressure wave; (**b**) forward and reflected pulse wave velocity relative to the velocity of blood flow with rotation speed (ω).

This is similar to the steepening of sea waves as they approach the shore. There are two causes of this non-linear effect. The first cause is the fact that the stress–strain curve for arterial walls is non-linear. Therefore, as pressure increases during systole, the vessel wall becomes more. The second cause occurs in the presence of reflected waves. The speed of the pulse wave (c) should really be measured relative to the local fluid speed (ν) rather than the stationary vessel wall. This means that the forward wave speed is ($c + \nu$) and the reflected wave speed is ($c - \nu$). This combination of speeds will also tend to steepen the acceleration phase of the systolic peak.

4.2. Gloomy Eyelet

The rotating mode shapes will be induced on the forced vortex region (Rigid Zone) of the Rankine model. While the speed of the vortex region will be increased, the pressure of fluid starts to drop as a ship can compress the space (like the spring) in front of the ship and stretch space (like the spring) behind the ship. Resonance can cause a rapid pressure drop (axial acceleration) to occur along with angular acceleration [10,12].

$$\alpha(t) = \beta(t) = \frac{\alpha(t)}{2} \Rightarrow \frac{d\omega}{dt} - 2\omega^2(t) = 0, \tag{5}$$

$$P_0 = P_\infty - \rho\omega^2 R_0^2 \Rightarrow P_0 = P_\infty - \rho\frac{d\omega}{dt}R_0^2, \tag{6}$$

$$\dot{\Omega} = \frac{d\Omega}{dt} = (\frac{-2}{\rho r_0^2})dp, \tag{7}$$

The possibility of quantified energy is studied in the gloomy eyelet. There is a standing wave in the pressure field caused by the rotating mode shape of the gloomy eyelet as below:

$$p_a(t) = -p'_a \cos(\omega_a t), \tag{8}$$

where p'_a the acoustic pressure amplitudes and $\omega_a = 2\pi/T$.

With these hypotheses, the particle energy is given by that of the particle in an infinitely deep well. As the particle remains to border in the gloomy eyelet. So, we can suppose a particle of mass subjected to a potential energy V(r) defined by:

$$\mathrm{V(r)} = 0 \qquad \text{pour} \quad -\mathrm{R} < \mathrm{r} < \mathrm{R}, \tag{9}$$

$$\mathrm{V(r)} = +\infty \quad \text{pour} \quad -\mathrm{R} < \mathrm{r} < \mathrm{R}, \tag{10}$$

The particle movement is one degree of freedom r and it is supposed that the particle makes one go with a constant velocity v, see Figure 4.

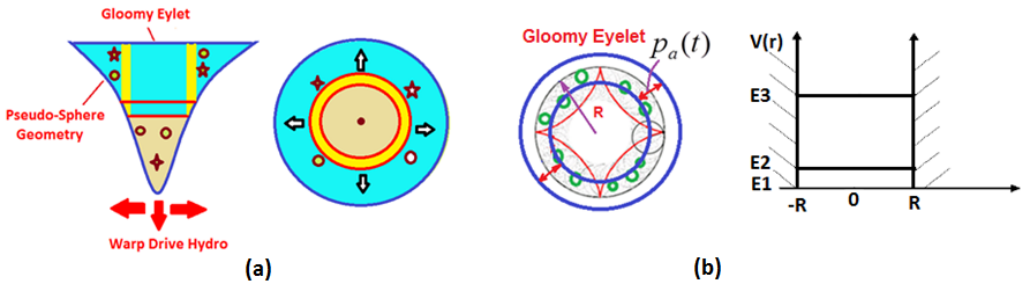

Figure 4. (**a**) Generation of gloomy eyelet and warp drive model on the pseudo-sphere geometry of pressure drop of Rankine model; (**b**) potential energy field for the gloomy eyelet inside the border line of gloomy eyelet on the standing wave of rotating mode shape.

The Planck's quantification condition gives:

$$\int pdq = 4m|v|R = nh, \tag{11}$$

With p impulse of the particle, q coordinated generalized, n integer or equal to one, h Plank constant. So, the total energy equal to the kinetic energy is:

$$E_{particle} = \frac{1}{2}mv^2 = \frac{n^2h^2}{32m_eR^2} \tag{12}$$

Equation (12) gives the particle quantified energy which moves on an axis of length equal to the diameter of the gloomy eyelet. The energy is a function of $1/mR^2$ [14].

It is predicted that the gloomy eyelet will appear in mediums such as left ventricular and DNA with assumed rotating frequency (ω). The beat pressure (standing wave) with the assumed frequency (Ω) can be generated by the pressure wave of blood on the blood vessel and the reflecting wave of blood pressure on the blood vessel. The beat frequency of the pressure vessel is anticipated around 1 Hz to 1.3 Hz.

A spring pendulum (also called elastic pendulum or swinging spring) is a physical system that can appear in gloomy eyelet (GE). DNA with a double helix can act as two swinging springs at the specific frequency of swinging motion.

The beat frequency (ω) of blood pressure on the blood vessel and the rotation of the left ventricular with speed (Ω) coincide together in the Rankine model. In this case, it leads to appearing as a sudden pressure drop and an accelerated cavity in the medium of the warp drive hydro model. This phenomenon is expected to occur in DNA and the swinging spring frequency (Ω) of the DNA approach to the beat frequency (ω) of blood pressure on the blood vessel possibly appears as a sudden pressure drop (accelerated cavity) based on the Rankine model. The medium including the gloomy eyelet moves toward particles and nanobubbles. This relative movement of the medium can generate a shock wave along with a pressure drop caused by passing through the sound speed in that medium.

It leads to a longitudinal increase in DNA and the creation of a cavity with a nanoscale with a drop in pressure in DNA. In this case, it is anticipated to appear in gloomy eyelet (GE) inside the WDH model in DNA. The gloomy eyelet has been presented in Figure 5.

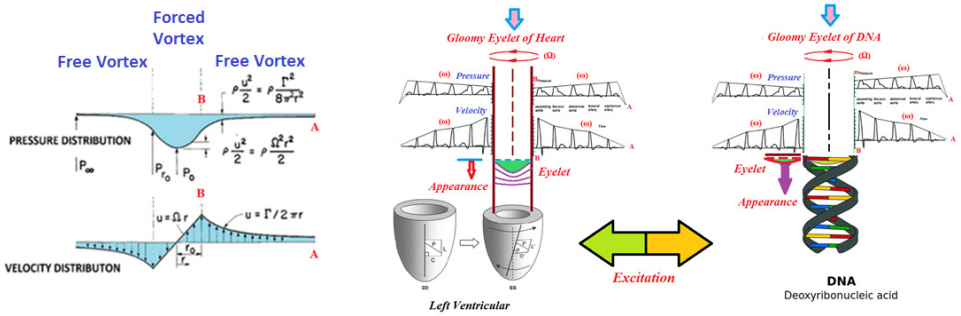

Figure 5. Gloomy eyelet (GE) generated by coinciding between the frequency (ω) of the beat wave of blood pressure of vessel with the frequency of DNA and the left ventricular (Ω) lead to the sudden pressure drop (accelerated cavity) of Rankine model (WDH model). The Rankine vortex model assumes a solid-body rotation (forced vortex) inside a cylinder of radius r (from the axis of rotation to point B) and a potential vortex (free vortex) outside the cylinder (between point A to point B).

Electrification in natural processes is unified through the quantum electrodynamics (QED) confinement of electromagnetic (EM) thermal kT energy of atoms in nanoparticles (NPs). NPs have EM confinement frequencies beyond the vacuum ultraviolet (VUV) that by quantum mechanics (QM) restricts the specific heat of the atoms to vanishing small levels, and therefore transient kT energy remaining after solids and liquids fragment or steady kT energy absorbed from molecular collisions in the surroundings cannot be conserved by an increase in temperature. Instead, conservation proceeds by the emission QED-induced nonthermal EM radiation that at VUV levels electrifies the natural process by the photoelectric effect [6,7].

In NPs, the EM confinement frequency f and wavelength of the QED-induced photons are,

$$f = c/ë \quad , \quad \lambda = 2Dn_r, \tag{13}$$

where c is the speed of light and nr is the refractive index of the N_P. The Planck energy E_p QED photons are,

$$E_p = \frac{hc}{2Dn_r}, \tag{14}$$

where h is Planck's constant.

N_P atoms are treated as harmonic oscillators having the dispersion of kT energy.

If the increase in N_P temperature is absent, the collisional Q_C heat is conserved by the emission of EM radiation,

$$E_p \frac{dN_P}{dt} = Q_C, \tag{15}$$

where dN_P/dt is the rate of QED photons produced having Planck energy E_P. The QED-induced current I is,

$$I = E_p \frac{dN_P}{dt} Ye, \tag{16}$$

where, Y is the electron yield/VUV photon, and e is the electron charge [15,16].

Photons can participate in the process of CMRF (co-moving reference frame) and tiny torsion of space–time inside the gloomy eyelet. Generally, these phenomena in gloomy eyelet (GE) reveal the tiny distortion of space–time inside gloomy eyelet (GE). The gloomy eyelet moves inside the trajectory of pseudo-spherical trajectory of warp drive hydro (WDH) model on the Rankine model.

A combination of the natural motion of DNA and the beat pressure inside the blood vessel can prepare the new and desirable condition for generating warp drive hydro (WDH) model on the Rankine model. DNA with a two-helix structure behaves similarly to a pseudo-spherical geometry.

Gloomy eyelet is made by the accelerated cavity due to sudden pressure drop on the WDH model. Resonance leads to forming pseudo-spherical trajectory and the gloomy eyelet and as well negative pressure. The photons caused by QED (quantum electro dynamic), the implosion of bubbles along with the radial, and axial motion of gloomy eyelet can be applied by the model of co-moving reference frame (CMRF). Photons can move in the different directions inside pseudo-sphere geometry and the gloomy eyelet.

In particular, the standing vibrational waves in the cavity may provide the necessary conditions for photon emission. The interaction of photons with phonons is a consequence of quantization for vibrational waves. Known as the dynamical Casimir effect, a cavity with accelerating boundaries generates photon pairs.

The photons caused by QED (Quantum Electro Dynamic) inside the gloomy eyelet (GE) can be formed and it can be applied by the model of co-moving reference frame (CMRF). Photons can move in different directions inside GE. The cavity of GE with accelerating boundaries generates photon pairs.

Special and general relativity were used to show that inertia arises out of the intimate relationship between the energy content of matter and the local structure of space–time. More specifically, the analysis showed that the inertial resistance force of a body undergoing uniform acceleration in flat, Minkowski space–time can be expressed as

$$\vec{F} = -E_0 \vec{\nabla}\left(\frac{dt}{d\tau}\right) = \overline{N}\hbar\nu_0 \nabla\left(\frac{dt}{d\tau}\right) \tag{17}$$

where E_0 is the rest-mass energy of the body, and $dt/d\tau$ expresses the distortion of time in the co-moving reference frame (CMRF) of the body relative to Minkowski space–time. It was pointed out that, as a given body accelerates under the influence of an external force, proper time in the CMRF of the body becomes increasingly distorted relative to time experienced by observers in Minkowski space–time.

It is assumed the cavity inside gloomy eyelet (GE) made by resonance acts as CMRF of the vessel, 'S'. The energy content will be $\overline{E}_0 = \overline{N}\hbar\nu_0$; E_0 resides in a region of space–time in which time is distorted according to $dt/d\tau$. The radiation pressure inside the cavity of gloomy eyelet (GE) and pseudo-sphere geometry will be [17]:

$$\Delta v_i = v_2 - v_1 = -v_0 r_{(cavity-GE)} \overline{\nabla}\left(\frac{\partial t}{\partial \tau}\right), \tag{18}$$

$$\vec{F}_r = \frac{h}{r_{cavity-GE}}(v_2 - v_1) = -h\nu_0 \overline{\nabla}\left(\frac{\partial t}{\partial \tau}\right), \tag{19}$$

$$\vec{F}_{GE} = -E_0 \vec{\nabla}\left(\frac{dt}{d\tau}\right) = \overline{N}\hbar\nu_0 \nabla\left(\frac{dt}{d\tau}\right), \tag{20}$$

The pseudo spherical trajectory caused by a pressure drop inside the warp drive acts as an impedance transformer. It is foreseen that the frequency of the rotating mode shape) coincide with the frequency of pseudo-spherical trajectory. The resonance phenomena can generate a fast pressure drop and the rotating speed in the vortex flow of gloomy eyelet. It is possible to create quasi-gravity due to negative pressure, CMRF inside the gloomy eyelet and between the parallel geodesics, and also the redshift of probable photons on the gloomy eyelet.

In these cases, forces and some waves can occur between particles inside gloomy eyelet. The external particle is exposed to quasi-gravity and adhesion, as well as new binding. The effective processes and their relationship in the creation of gloomy eyelet have been presented in Figure 6.

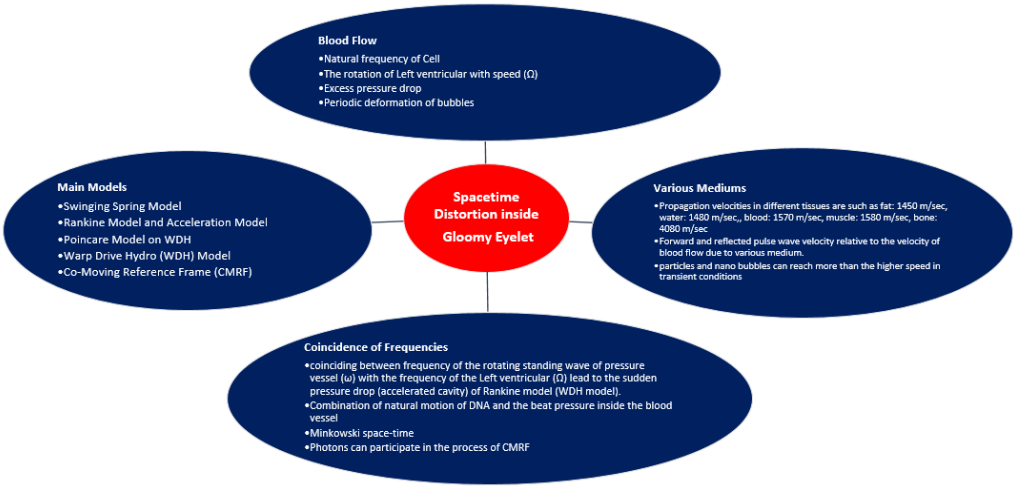

Figure 6. Effective processes and their relationship in the formation of gloomy eyelet inside the cell nucleus.

5. Study of New Interactions

It seems that the changes and effects over the gloomy eyelet in the cell nucleus can cause the appearance of unforeseen phenomena in the sensitive systems of the human body. It is possible to study some interactions as follows:

- The wireless systems revolution has generated a wave of innovative results that dramatically expand the availability of voice and data almost anywhere. While this change has significantly broadened the possibility for new and better wireless communication ends, it has proffered further considerations for antenna design concepts. The control of specific absorption rate (SAR) is a crucial factor that should be equally considered alongside traditional antenna design parameters. The absorption of electromagnetic energy (EM) emitted from the cellular phone has been considered in recent years. The specific absorption rate is a defined parameter for evaluating power deposition in human tissue. For mobile phone compliance, the SAR value must not exceed the exposure guidelines, 2 watts per kilogram (W/kg) [18]. Gloomy eyelet theory can influence the control of specific absorption rate (SAR).
- A narrative review of research literature has been studied to "map the landscape" of the mechanisms of the effect of sound vibration on humans, including the physiological, neurological, and biochemical. It begins by narrowing music to sound and sound to vibration. The focus is on low-frequency sound (up to 250 Hz) including

infrasound (1–16 Hz). Types of applications are described and include whole-body vibration, vibroacoustics, and focal applications of vibration. The literature on mechanisms of response to vibration is categorized into hemodynamic, neurological, and musculoskeletal. Basic mechanisms of hemodynamic effects including the stimulation of endothelial cells and vibropercussion; neurological effects including protein kinases activation, nerve stimulation with a specific look at vibratory analgesia, and oscillatory coherence; musculoskeletal effects including muscle stretch reflex, bone cell progenitor fate, vibration effects on bone ossification and resorption; and anabolic effects on the spine and intervertebral discs [19]. Gloomy eyelet can improve the field of vibrational medicine.

- At the microscopic level, in the mammalian nervous system, conduction delays (latencies) along one axon vary widely, from less than 100 is to more than 100 ms. As in an electrical network, the latency is the ultimate parameter that determines the amount of data that can be transferred over a time period. Those latencies depend, obviously, on the axon length, but, counterintuitively, more on the axon diameter [20]. Now, there is a possibility that latencies can be dependent on gloomy eyelet.

6. Conclusions

The effects and traces of frequency responses of human body organs such as delays, interactions, and also the new connections between body cells with each other can be examined by warp drive hydro and gloomy eyelet models. There are two main issues individual tiny distortions of space–time inside the infinity of cells and the relation between the individual distortions of space–time in the various cells. There is a possibility that the specific frequencies inside the human body can create the continuity between individual distortions of space–time. In this case, we will be facing a new integrated environment with complex and unknown behavior along with the new various phenomena. Interaction between buoyancy due to gloomy eyelet (GE) and gravitational force can be applied for the analysis of some unknown phenomena that occurs in living beings. It seems that the existence of tiny distortions of time and gloomy eyelet can be considered as other required phenomena inside human cells and the change in the initial tiny space–time can generate unforeseen conditions in the cells.

Author Contributions: Conceptualization, methodology, formal analysis, investigation, writing-original draft preparation—F.A.; reviewed and editing—J.-M.S. All authors have read and agreed to the published version of the manuscript.

Funding: This research received no external funding.

Conflicts of Interest: The authors declare no conflict of interest.

References

1. Benjamin, A.; Zubajlo, R.E.; Dhyani, M.; Samir, A.E.; Thomenius, K.E.; Grajo, J.R.; Anthony, B.W. A Novel Approach to the Quantification of the Longitudinal Speed of sound and its potential for Tissue Characterization (Part-I). *Ultrasound Med. Biol.* **2018**, *44*, 2739–2748. [CrossRef] [PubMed]
2. Zarandi, M.M.; Bokdar, A.; Stiharuz, I. Investigations on Natural Frequencies of Individual Spherical and Ellipsoidal Bakery Yeast Cells. In Proceedings of the COMSOL Conference 2010, Boston, MA, USA, 7–9 October 2010.
3. Wienke, B.R.; O'Leary, T.R. *RGBM Algorithm Overview: Concepts, Bases, Validation, Testing and References*; American Diving and Marine; Los Alamos National Laboratory: Egg Harbor Township, NJ, USA; Santa Fe, NM, USA, 2004.
4. Arora, D.; Behr, M.; Pasquali, M. *Blood Damage Measures for Ventricular Assist Device Modeling*; Rice University: Houston, TX, USA, 2003.
5. Kolandavel, M.K.; Fruend, E.T.; Pederson, E.M.; Ringgaard, S.; Walker, P.G. A CFD Study of the Effects of Physiological Vessel Wall Motion on Oxygen Transport in Coronary Arteries. Available online: http://fluid.ippt.gov.pl/ictam04/text/sessions/docs/FM1/11851/FM1_11851.pdf (accessed on 17 November 2022).
6. Petrov, G.A. Rotation of the Apparent Vibration Plane of a Swinging Spring at the 1:1:2 Resonance. *Mech. Solids* **2017**, *52*, 243–253. [CrossRef]
7. Pokorny, P. Stability Condition for Vertical Oscillation of 3-dim Heavy Spring Elastic Pendulum. *Regul. Chaotic Dyn.* **2008**, *13*, 155–165. [CrossRef]

8. Aarønes, T.E. Study of the Natural Frequencies of a Disc. Master's Thesis, Norwegian University of Science and Technology, Trondheim, Norway, 2015.
9. Mehdigholi, H. Forced Vibration of Rotating Discs And Interaction With Non-Rotating Structures. Ph.D. Thesis, Imperial College of Science, Technology and Medicine, University of London, London, UK, April 1991.
10. Darzin, P.G.; Riely, N. *The Navier-Stokes Equations: A Classification of Flows and Exact Solutions*; Cambridge University Press: Cambridge, UK, 2006.
11. Choi, J.-K.; Chahine, G.L. Non-spherical Bubble Behavior in Vortex Flow Fields. *Comput. Mech.* **2003**, *32*, 281–290. [CrossRef]
12. Hsiao, C.T.; Chahine, G.L. Numerical Simulation of Bubble Dynamics in a Vortex Flow Using Navier Stokes Computation and Moving Chimera Grid Scheme. In Proceedings of the CAV 2001: Fourth International Symposium on Cavitation, Pasadena, CA, USA, 20–23 June 2001.
13. Geneste, F.J. LENR: From Experiment to Theory. Airbus Group, Presented at the Conference that Was Hosted by Airbus in Toulouse. 2015. Available online: https://e-catworld.com/2015/10/17/lenr-from-experiment-to-theory-paper-by-jean-francois-geneste-airbus-group/ (accessed on 17 November 2022).
14. Maiga, M.A.; Adama, M. Single Bubble Sonoluminescence of particles model. *arXiv* **2012**, arXiv:1212.1083.
15. Prevenslik, V.T. Flow Electrification by Cavity QED. Available online: http://www.esdjournal.com/techpapr/prevens/flow1.pdf (accessed on 17 November 2022).
16. Prevenslik, T. A Unified Theory of Electrification in Natural Process. Available online: https://www.academia.edu/68612562/A_Unified_Theory_of_Electrification_in_Natural_Processes (accessed on 17 November 2022).
17. Ridgely, T.C. On the Origin of Inertia. Available online: https://citeseerx.ist.psu.edu/document?repid=rep1&type=pdf&doi=587322c845d655f598470f51804c3f9d56caca39 (accessed on 17 November 2022).
18. Karimian, R.; Ahmadi, S.; Ardakani, M.D.; Zaghloul, M. Human Body Specific Absorption Rate Reduction Employing a Compact Magneto-Dielectric AMC Structure for 5G Massive-MIMO Applications. *Eng* **2021**, *2*, 501–511. [CrossRef]
19. Bartel, L.; Mosabbir, A. Possible Mechanisms for the Effects of Sound Vibration on Human Health. *Healthcare* **2021**, *9*, 597. [CrossRef] [PubMed]
20. Le Bihan, D. On time and space in the brain: A relativistic pseudo-diffusion framework. *Brain Multiphys.* **2020**, *1*, 100016. [CrossRef]